Flow and dispersion through a close-packed fixed bed of spheres

A. M. Reynolds,* S. V. Reavell, and B. B. Harral
Silsoe Research Institute, Wrest Park, Silsoe, Bedford MK45 4HS, United Kingdom
(Received 14 March 2000)

Fluid flow through a close-packed fixed bed of spheres in a face-centered cubic arrangement is investigated in numerical simulations using a lattice-Boltzmann formulation. The dispersion of a tracer gas is studied both experimentally and numerically. At low Reynolds numbers, Re$\leqslant$14, the flow is steady with a distribution of normalized local kinetic energies that follows a power law over roughly three orders of magnitude. Consequently the ''stagnant'' zones play a significant role in determining transport through the packed bed in contrast with the dangling ends for the analogous electrical transport problem, where the distribution of local currents is log binomial. At higher Reynolds numbers transitions to time-oscillatory and chaotically (turbulently) varying flows are predicted to occur with a crossover to a log-normal distribution of local kinetic energies. At the onset of transverse velocity fluctuations the simulated trajectories of tracer particles can cross planes of symmetry, resulting in an abrupt enhancement of dispersion. The dispersion of tracer particles in the time-oscillatory and chaotic varying flows is predicted to be Fickian in the far field. Model predictions for dispersion in a chaotic flow with Re$\sim$100 are shown to be in good agreement with experiment.

PACS number(s): 47.55.Mh, 47.27.−i, 87.15.−v

I. INTRODUCTION

This paper reports on numerical studies of fluid flow through a close-packed fixed bed of spheres in a face-centerd-cubic arrangement. Also investigated, both experimentally and numerically, is the dispersion of tracer gas. Understanding flow and dispersion through packed-beds is of importance in several technological processes (e.g., filtration, catalysis, and chromatography). It could, for example, lead to improved practices in the food industry where chemical agents are applied to stored produce, such as potatoes, grain, and fruit.

Attention is focussed primarily on flows with Reynolds number, $\mathrm{Re}=Ua/\nu$ up to about 100, where a is the sphere radius, U is the average velocity throughout the bed, and ν is the kinematic viscosity of the fluid. In contrast with the much studied [1–4] low-Reynolds-number limit (Re$\ll$1), where the flow is stationary and where dispersion is dominated by molecular diffusion, flow and dispersion at moderate Reynolds numbers has received little attention. A notable exception is the experimental study of Wigner *et al.* [5] who, by observing a dye tracer released at the surface of a single sphere in a packed bed, noted a transition to unsteady flows for Re in the range 45–60. Transitions to unsteady flows have also been observed in numerical simulations of flows through packed beds of spheres [6] and in numerical simulations of two-dimensional flows through periodic and random arrays of aligned cylinders [7].

To simulate moderate Reynolds numbers flows, we will use a lattice-Boltzmann formulation. This method has been tested by comparing its predictions for a wide variety of Stokes flow problems with the results of a multipole method and by comparing the predictions for finite-Reynolds-number flows past a single row of cylinders and through a cubic array of spheres with finite difference results [8]. Currently, it is the only means of accurately predicting flows in complex three-dimensional geometries. Of particular interest will be the distributions of local kinetic energy that can have important implications for transport through the packed bed and the transition from steady to turbulent flow.

The experimental setup used to investigate the dispersion of a tracer gas is described in Sec. II. This is then followed in Sec. III by a brief description of the lattice-Boltzmann formulation and the numerical simulation of tracer-gas dispersion. Predictions for the fluid flow and dispersion of a tracer gas are discussed in Sec. IV. The experimental measurements of the mean concentrations along with comparisons with model predictions are then presented in Sec. V. Conclusions are drawn in Sec. VI.

II. EXPERIMENTAL SETUP

The experimental set up is shown schematically in Fig. 1. It is comprised of closely packed polystyrene spheres, with an approximate diameter of 45 mm, in a face-centerd-cubic (fcc) arrangement with a principal axis in the $x=y=z$ direction. This was achieved by first forming a close-packed horizontal layer of spheres; those centers form a triangular lattice. In the centers of these triangles a second layer of closely packed spheres was then fitted. The addition of a third layer is now possible in two different ways: either the spheres may be placed in the triangles of the second layer so that each sphere in the third layer is directly above spheres in the first layer or they may be placed in an alternative position which is not directly above the first layer. The former type of structure is that of a close-packed-hexagonal arrangement, while the latter is the fcc structure. The fcc structure was adopted because unlike the hexagonal arrangement there are no direct channels for dispersion orientated along the gradient in applied pressure, which runs from the top to the bottom of the arrangement. The packed bed consisted of 16 layers, with the

*Corresponding author. FAX: +44 (0)1525 860156. Electronic address: andy.reynolds@bbsrc.ac.uk

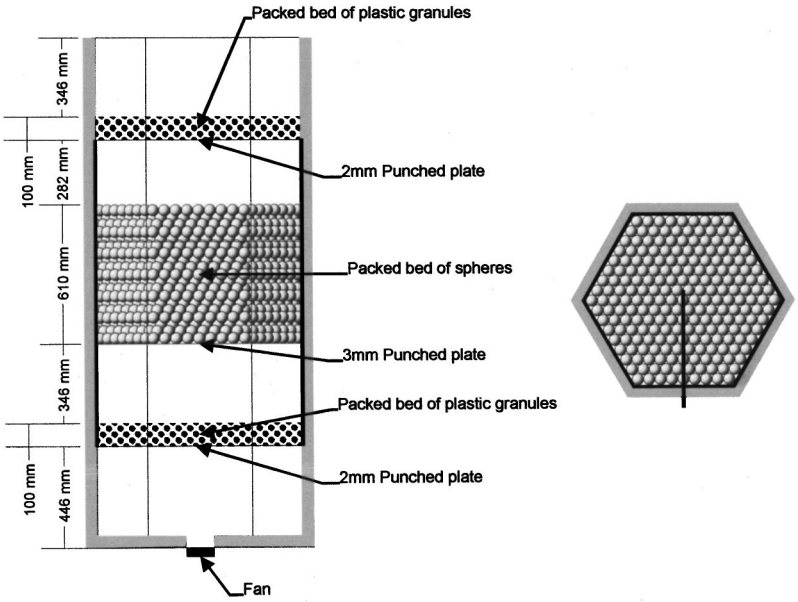

FIG. 1. Schematic representation of the experimental setup. Also shown is the line located 20 mm below the first layer of spheres along which measurements of gas concentration were made.

spheres in the 16th layer lying directly above those in the first layer.

The pack bed was enclosed within a hexagonal vessel, with across-corners width equal to 17 sphere diameters, constructed from plywood, and lined with a flexible polymer-based material into which the contact surfaces of adjacent spheres could be imbedded, thus preventing leakage of air and tracer gas there. The first and corresponding equivalent layers consisted solely of whole spheres whilst in the second, third, and corresponding equivalent layers partial spheres were required adjacent to the inside of the vessel to maintain constant packing density and arrangement and to prevent leakage. The bottom of this packed bed was held in place by a punched plate having holes of diameter 3 mm with centers regularly spaced at 5-mm intervals in a triangular arrangement.

The influence of the surroundings on the air flow through the rig was reduced by the placement of two closely packed beds of plastic granules with approximate diameter 3.5 mm, above and below the bed, and by conducting the experiments within a closed temperature-controlled room. Air was sucked through the arrangement using an electric fan and the resulting pressure difference across the packed bed of 2 Pa was monitored using an inclined manometer. The upper bed served to make uniform the air flowing into the packed bed of spheres.

A tracer gas (SF_6) was released continuously and isokinetically as a SF_6-air mixture (10% SF_6 by volume) at 0.2 $\mathrm{ml\,s^{-1}}$ from a pipe with internal diameter $\sim$3 mm, at a height of about 1.5 mm above the central sphere in the 16th (top) layer. SF_6 has a density of $\rho = 6.26\,\mathrm{kg\,m^{-3}}$ and is nonbuoyant. SF_6 was chosen as the tracer gas because of ease of detection. The effects of nonbuoyancy are not expected to be significant as the predicted settlement time is much longer than transport times due to advection by the fluid.

The concentrations of gas emerging from the packed bed was then measured and recorded at a height 20 mm below the first (bottom) layer, along the line depicted in Fig. 1. The sampler continuously drew off the tracer-gas-air mixture at a flow rate equal to the velocity of the air flow. The sampler had a response time of 1 s and a recovery time of 2 s. Statistically stationary profiles of mean gas concentration were obtained from 3-min time histories of measured concentration. Measured concentrations are accurate to within $\pm 2\%$.

III. NUMERICAL SIMULATIONS

A. Lattice-Boltzmann simulations

This section provides a brief description of the lattice-Boltzmann method (LBM) and its application to the simulation of flows through close-packed beds of spheres. More detailed descriptions of the particular lattice-Boltzmann (LB) formulation adopted, commonly denoted by D_3Q_{15}, can be found in Qian *et al.* [9] and Chen and Doolen [10].

In the LBM, a discrete analog of the linearized Boltzmann equation

$$f_i(\mathbf{x}+\mathbf{c}_i, t+1) - f_i(\mathbf{x},t) = -\frac{1}{\tau}[f_i(\mathbf{x},t) - f_i^{\mathrm{eq}}(\mathbf{x},t)] \quad (1)$$

is solved for the number density of molecules at node $\mathbf{x}$ at time t, $f_i(\mathbf{x},t)$, of a gas of ''fictitious'' molecules that translate from node to node on a cubic lattice with a discrete set of velocities $\mathbf{c}_i$. In the present model there are six velocities of speed 1 corresponding to the (100) directions, eight velocities of speed $\sqrt{3}$ corresponding to the (111) directions and one ''rest'' particle of speed 0. The distribution $f_i(\mathbf{x},t)$ is related to the fluid density ρ and the momentum density, $\mathbf{j} = \rho\mathbf{u}$, by

$$\rho = \sum_i f_i, \quad \mathbf{j} = \sum_i f_i c_u \quad (2)$$

and the nondimensional kinematic viscosity of the fluid ν is related to the nondimensional relaxation time τ by $\nu = (2\tau$

$-1)/6$. Appropriate forms for equilibrium distributions, $f_i^{\mathrm{eq}}(\mathbf{x},t)$, are taken from Qian *et al.* [9],

$$f_i^{\mathrm{eq}} = t_i\rho\left(1+\frac{1}{c_s^2}(\mathbf{c}_i\cdot\mathbf{u})+\frac{1}{2c_s^2}(\mathbf{c}_i\cdot\mathbf{u})^2-\frac{1}{2c_s^2}u^2\right), \quad (3)$$

where $t_i=2/9$ for rest particles, 1/9 for particles with speed 1, and 1/72 for particles with speed $\sqrt{3}$. The speed of sound $c_s=1/\sqrt{3}$.

Experimental measurements of dispersion, presented in Sec. V, indicate that the dispersion of the tracer gas did not extend significantly in the lateral direction beyond about three sphere diameters from the release position. This is much less than the half-width of the experimental rig, indicating that edge effects, arising from the finite size of the packed bed, can be neglected. Consequently in the numerical simulations the packed bed can be taken to extend infinity in all directions. This was implemented by modeling only flow within the basic fcc unit cell, subject to periodic boundary conditions. The difficulties associated with comparing predictions for dispersion *within* the packed bed with the measured dispersion beneath the bed is discussed later, in Sec. V.

The pressure does not vary significantly across the unit cell and so its effects are well approximated by a constant body force $\mathbf{F}$. This was implemented by calculating the equilibrium distribution functions with an altered fluid velocity $\mathbf{u}+\tau\mathbf{F}/\rho$, rather than with the actual fluid velocity $\mathbf{u}$ [11].

Each solid sphere is defined by a spherical surface which cuts some of the links between the lattice nodes. The fictitious gas molecules moving along these links were reflected so that, in a single time step, they return to the lattice nodes from where they came with an opposite velocity. As a result a no-slip velocity condition is imposed midway along the link. It is this easy implementation of the no-slip velocity condition by the ''bounce-back boundary scheme'' which makes the LBM ideal for simulating fluid flows in complicated geometries. The bounce-back scheme is, however, only first order in numerical accuracy at the boundary [12] and so degrades the LBM which for the interior nodes is second order in numerical accuracy. Bounce-back schemes that are second-order accurate have been proposed [13] but cannot be readily implemented for complicated geometries. For this reason they are not employed here.

The discrete representation of the spheres becomes more spherical with the increasing sphere-radius-to-node spacing ratio. However, the size of the lattice required to obtain accurate results is primarily controlled by the need to resolve the flow within the voids between neighboring spheres. The results of numerical simulations indicated that when void cross-sectional areas (approximately triangular in shape) contained more than about $\frac{1}{2}\times25\times25$ nodes, grid independent results (errors of less than 5%) were obtained for $\mathrm{Re}<120$. This was achieved by having $100\times100\times100$ nodes within a unit cell. The maximum mean velocity was less than the speed of sound thus ensuring incompressible fluid dynamics.

The initial value problem was solved in which the fluid velocity was zero throughout the domain and a body force was applied at time $t=0$. In the case of periodic solutions, the calculations were continued until the mean flow (averaged over the flow domain) at successive equivalent times within the cycle varied by less than 0.01%. Quasiperiodic (i.e., flows which did not display periodicity on the time scales of the simulations but which had a discrete Fourier spectrum) and chaotic solutions were taken to be converged when both the mean flow and the velocity variance varied by less than 1% during the last 25% of the run. Typically, 200 000 time steps were required. It should be noted here and throughout the paper that because of the difficulties associated with the correct identification of quasiperiodicity, the term ''quasiperiodicity'' is used in the aforementioned sense which does not distinguish between the strict definition of quasiperiodicity in terms of a finite number of incommensurate Fourier modes and time histories containing many different commensurate modes.

B. Simulation of particle trajectories

There are two possible approaches to the modeling of particle dispersion. In the Eulerian approach a diffusion-advection equation for the time evolution of a scalar is solved whilst in the Lagrangian approach mean concentrations of a scalar are calculated by ensemble averaging over the simulated single independent tracer-particle trajectories. In this study the Lagrangian approach is adopted because the boundary conditions do not need to be specified *a prori* in an *ad hoc* fashion, the approach does not introduce numerical diffusion, and because it can be readily extended to ''heavy'' and Brownian particles.

The trajectories of tracer particles $(\mathbf{x}_p,\mathbf{u}_p)$ were simulated by numerical integration of the tracer advection equation

$$\frac{d\mathbf{x}_p}{dt}=\mathbf{u}_p(\mathbf{x}_p,t), \quad (4)$$

where to filter out the effects of the staggered momentum, inherent in the solution to the D_3Q_{15} model [14], the particle velocity $\mathbf{u}_p$ is taken to be the local fluid velocity, temporal averaged over two successive iterations of the lattice Boltzmann model. This quantity is known only at the nodes of the computational grid and at discrete times. An approximation to this quantity at the particle location at time t was obtained by linear interpolation from the grid nodes to the particle location and from the solutions for times t' and $t'+1$ to time t where $t'\leqslant t<t'+1$.

Close to the boundaries the spatial resolution of the grid is not sufficient, nor can it ever be, for an accurate determination of particle trajectories. These inaccuracies, which are compounded by the interpolation, can result in the nonphysical deposition of some tracer particles. To overcome this difficulty the flow at the boundary nodes, which is predicted to vanish, was given a small normal outward component. The magnitude of this normal component was taken to be constant throughout the flow domain, equal to the smallest value which prevented all nonphysical deposition. This was typically two or more orders of magnitude less than the magnitude of the velocity at the nearest node within the flow. The simulated trajectories of tracer particles were found to be insensitive to a tenfold increase in the value of the outward velocity component.

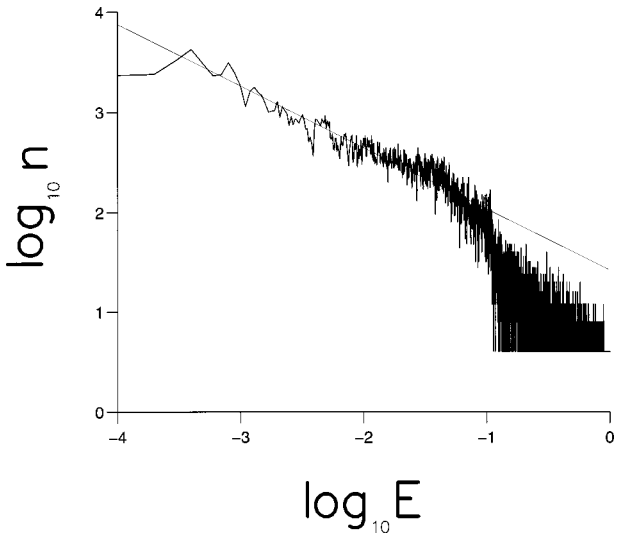

FIG. 2. The distribution of normalized local kinetic energy for a steady flow with Re≪1.

IV. PREDICTED FLOWS AND TRACER-PARTICLE DISPERSION

The nature of the flow, whether steady, time oscillatory, or chaotic depends on the Reynolds number Re. Here Re is based on the radius of a sphere and the magnitude of the volumetrically and temporally averaged fluid velocity within the voids. The root mean square (rms) of the magnitude of the volumetrically averaged fluid velocity is used to define a second Reynolds number Re′, characterizing the temporal fluctuations in velocity.

For low Reynolds numbers, Re≤14, the fluid flow is predicted to be steady but very complex due to the complex geometric structure of the packed bed which creates very tortuous pathways for fluid flow. A natural quantity to statistically characterize the fluid flow associated with each node in the computational grid is the kinetic energy, $k = 1/2\rho\mathbf{u}\cdot\mathbf{u}$. Figure 2 shows that the distribution of normalized kinetic energy $E = k/k_{\max}$, where $k_{\max}$ denotes the maximum kinetic energy. It is seen that over roughly 3 orders of magnitude ($10^{-4} < E < 10^{-1.5}$) the distribution $n(E)$ of E follows a power law with $n(E) \sim E^{-\alpha}$, where $\alpha = 0.64 \pm 0.05$. Intriguingly, the same exponent, $\alpha = 0.64 \pm 0.05$, was found [15] to characterize the distribution of E in the Stokes flow forming the ''conducting backbone'' at the threshold of percolation in two-dimensional random porous media. Andrade *et al.* [15] suggested that this power law distribution indicates that the local kinetic energy is sensitive to the geometry of the pore structure. Consequently, the ''stagnant'' zones play a significant role in transport through the packed bed, in contrast with the dangling ends for the analogous electrical transport problem [16,17].

In addition to the steady flows, six other flows were simulated: a flow with Re≈15.4, which was time periodic in the direction of the applied pressure gradient and steady in the transverse directions; flows with Re≈19.8 and Re≈22.0 which were time periodic in both the longitudinal and transverse directions; a ''quasiperiodic'' flow with Re≈29.5; and chaotic (low-Reynolds-number turbulent) flows with Re ≈42 and Re≈113. Characteristic features of the these flows are shown in Fig. 3.

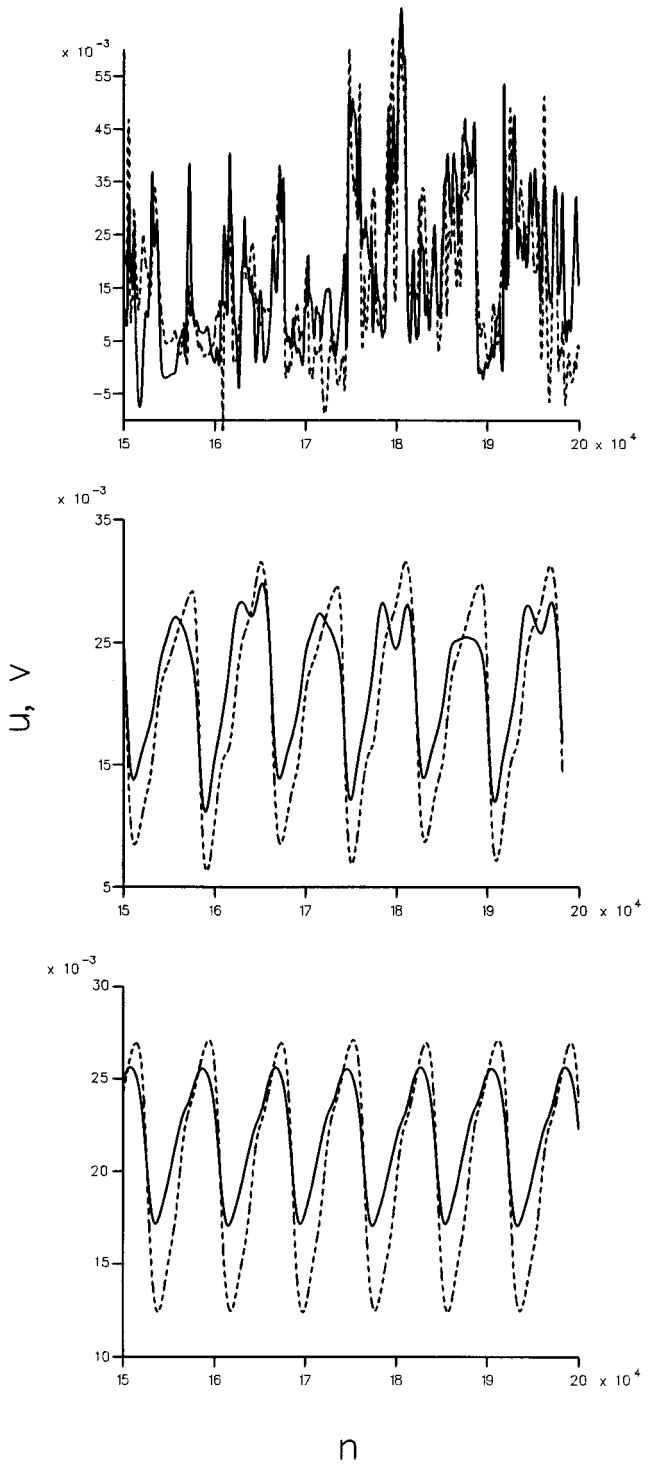

FIG. 3. Predicted fluid velocities histories at (0.5,0,0) for a periodic flow with Re≈22.0 (bottom), a quasiperiodic flow with Re ≈29.5 (middle), and a turbulent flow with Re≈113 (top). The u and v components of velocity after n iterations of the LBM are indicated by solid and dashed lines, respectively. To remove the ''staggered momentum,'' velocities have been averaged over two successive iterations.

The corresponding phase diagram is shown in Fig. 4. The same sequence of transitions but with different critical Reynolds numbers has also been reported by Hill and Koch [6] who used a LBM to simulate flows through packed beds of spheres in a fcc arrangement with the gradient in applied

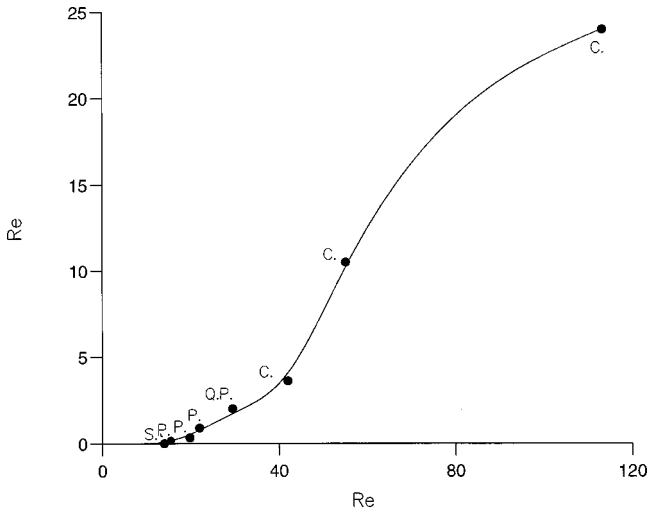

FIG. 4. Phase diagram. Calculations are presented by solid dots. The solid line serves only as a guide for the eye. The symbols *S*, P_L, *P*, Q. P., and *C* denote flows which are stationary, time periodic in the longitudinal direction, time periodic in both the longitudinal and transverse directions, quasiperiodic, and chaotic.

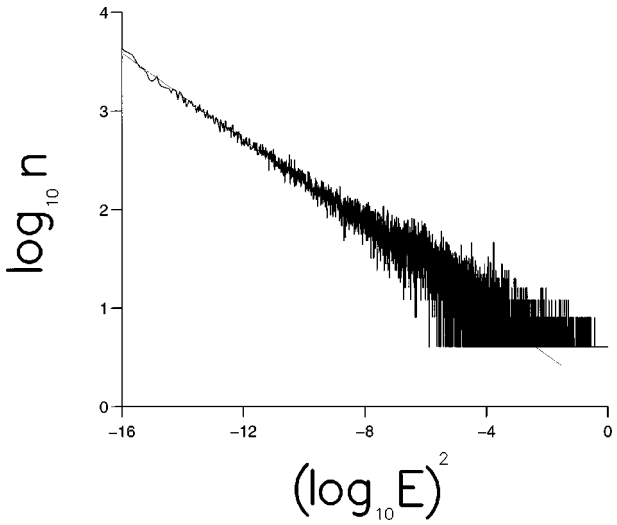

FIG. 5. The distribution of normalized local kinetic energy for a chaotic flow with Re≈113.

pressure to be in the on-axis (100) direction. For this case, unsteadiness first occurs at Re≈32.4 [18]. This indicates that the on-axis flow is more stable than the (111) flow. For close-packed arrangements of spheres it is the large velocities in the gaps rather than symmetry breaking of the flow about any single sphere due to the velocity disturbances of the other spheres or wake instabilities which destabilize the flow. The velocity in the gaps is related to the reciprocal of the effective cross-sectional area of the gap, which is $(\sqrt{3}-\pi/2)R^2$ when the applied gradient in pressure is the (111) direction and $(4-\pi)R^2$ when it is in the (100) direction, where *R* is the sphere radius. The critical Reynolds number for the (111) direction can therefore be expected to be approximately $(\sqrt{3}-\pi/2)/(4-\pi)\approx 5.3$ smaller than for the (100) direction, which is not too dissimilar from the results of the numerical simulations.

Although the results of numerical simulations suggest that the branch of the phase diagram identified in Fig. 4 is robust to perturbations with amplitudes large compared to the amplitude of the flow oscillations, it is possible that other less-stable branches also exist, as is the case when the applied pressure is in the (100) direction [18]. There was no indication of their being any period-multiplying transitions, in stark contrast with the results of numerical simulations using a LBM for two-dimensional flows through periodic arrangements of cylinders [7]. Koch and Ladd [7] reported observing period doubling when the pressure gradient is near the primary axis and transitions to odd multiples when the pressure gradient is along the diagonal of the array.

Figure 5 shows that in contrast with the steady flow, the normalized local kinetic energy of the chaotic flow has a log-normal distribution over roughly 3 orders of magnitude in analogy with the log-binomial distribution for the local currents found in the corresponding random resistor network [16,17]. The distinction between the binomial distribution and the familiar Gaussian approximation is only of importance when calculating higher moments. This arises because the moments are actually exponential moments when all quantities are expressed in terms of the fundamental variable $x=\ln k/\ln k_{\max}$. The log-normal distribution leads naturally to an infinite set of exponents being required to describe the moments of kinetic energy. Consequently in stark contrast with the steady flow case, the kinetic energy distribution cannot be characterized by a unique velocity scale.

Several factors may contribute to the dissimilarities between the scaling of the steady and turbulent flows. At low values of Re, there is a tendency for the fluid at the local void scale to preserve the parabolic shape of the velocity profiles even when the fluid is confined to very tortuous pathways. At high values of Re, however, the irregular geometry is very effective in producing sudden and dramatic changes in the directions and magnitudes of the fluid velocities, thus distorting their parabolic profile at the local level of the void space. Furthermore, at high values of Re the nonlinear advection term in the Navier-Stokes equations become relevant and can lead to vortices and flow separation. An example of the energy-frequency spectra $S(\omega)$ for the chaotic velocity fluctuations is shown in Fig. 6. The spectra has a dissipation range characterized by $S\sim\omega^{-5}$ and there is some suggestion of an inertial subrange, where over a narrow range of frequencies, $S\sim\omega^{-5/3}$. The absence of a well-defined inertial subrange is not surprising given the low Reynolds number of the flow and the strong anisotropy of the larger scales of motion coupled with the presence of a gradient in the mean flow [19].

In the absence of molecular diffusion, tracer particles emitted from a point source into a steady flow cannot disperse whilst for the time-oscillatory flows, tracer-particle dispersion is severely constrained because there cannot be any transport across planes of symmetry. However, there can be transport of tracer particles across planes of symmetry when the transverse component of fluid velocity fluctuates because then the instantaneous velocity field is no longer constrained by symmetry. Thus, an abrupt increase in dispersion is predicted to accompany the onset of transverse velocity fluctuations.

The predicted dispersion of tracer-particle trajectories in a time-oscillatory flow with Re≈22 is shown in Fig. 7. The anisotropy of the dispersion arises primarily from the par-

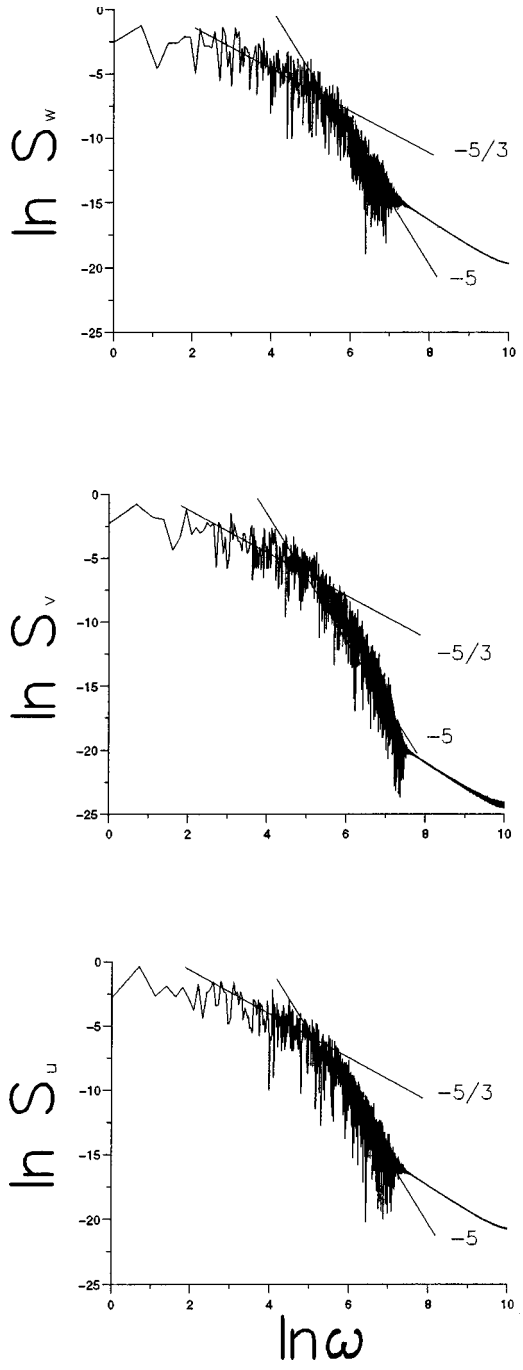

FIG. 6. Energy-frequency spectra $S(\omega)$ for the velocity fluctuations at (0.5,0,0) in the chaotic flow with Re≈113. Inertial subranges and dissipation ranges are indicated.

ticular time-oscillatory mode of the flow realized in the numerical simulations. Two components of this flow have dissimilar amplitudes, indicating that at least two such unsteady modes are possible. The anisotropy is also a consequence of the periodicity of the tracer-particle tracks, a Lagrangian property of the fluid, being different from the periodicity of the Eulerian flow. This can arise when both the streamwise and lateral components of velocity are unsteady. Figure 8 shows that in the far field the rms spread of tracer particles σ closely follows a power law $\sigma \sim d^{\beta}$, where d is the distance from the source measured along the center line of the plume (i.e., measured normal to the horizontal planes of spheres).

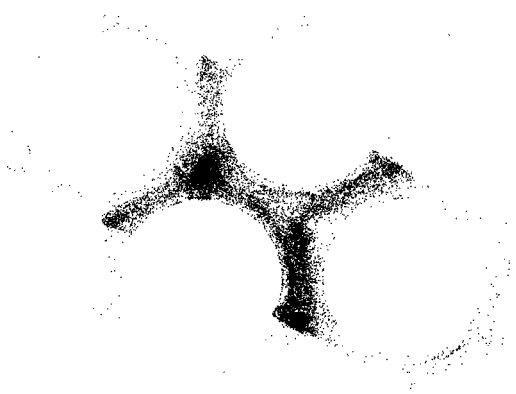

FIG. 7. Locations in the plane containing the lower poles of spheres in the first layer through which the simulated trajectories of tracer particles passed for a time-oscillatory flow with Re≈22.0. The particles were released from a continuous source located just above the central sphere in the 16th layer.

For the major axis of lateral dispersion $\alpha = 0.51 \pm 0.01$ whilst for the minor axis $\beta = 0.3 \pm 0.01$. The far-field dispersion is not, however, anomalous but Fickian, i.e., $\sigma^2 \propto t$ where t is the transit time.

For the chaotic flow with Re≈113, the spread of tracer particles becomes isotropic beyond the third horizontal plane of spheres beneath the source and $\sigma \sim d^{1/2}$, as shown in Fig. 8. In the far field diffusion is again Fickian and so, contrary to most cases of dispersion in inhomogeneous turbulence, can be described by a diffusion-advection equation. This Fickian characteristic is most probably a consequence of the length scales and time scales on which transport occur being much larger than the scales of variations in the velocity field experienced by the tracer particles. In this context it is noteworthy that dispersion due to molecular diffusion in Stokes flows through porous media is also predicted to be Fickian [3,20].

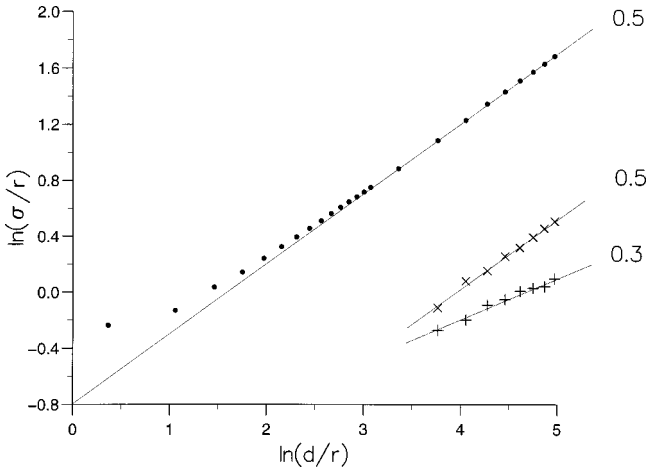

FIG. 8. The rms spread of tracer particles σ in a periodic flow with Re≈22 (×, major axis of lateral dispersion; +, minor axis of lateral dispersion) and the chaotic flow with Re≈113 (●). Distances d are measured from the source in the direction normal to the horizontal planes of spheres. Model predictions are shown for dispersion on the horizontal planes (between the first and 100th) containing the centers of the spheres. The power-law regimes $\sigma \sim d^{0.5}$ and $\sigma \sim d^{0.3}$ are indicated.

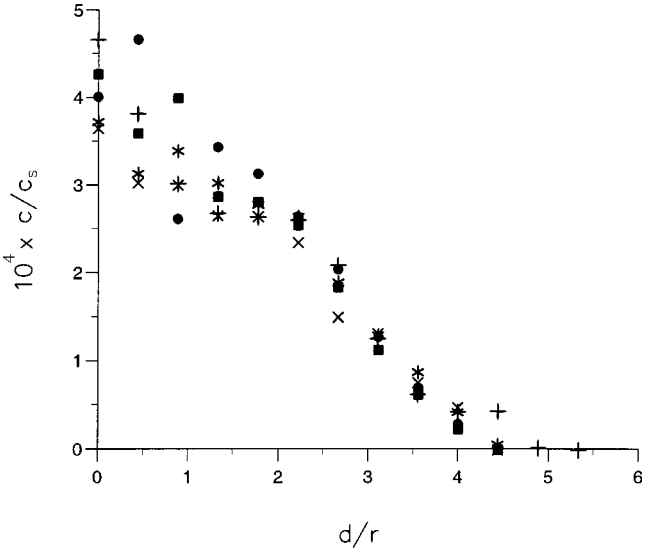

FIG. 9. Six replicate profiles of mean concentrations c measured 20 mm below the lower poles of the spheres in the first layer. Distances d are measured from the central sphere in the first layer along the line shown in Fig. 1. The source strength is denoted by c_s and the sphere radius by r. Measured concentrations are accurate to within $\pm 2\%$.

Numerical instabilities inherent in the LB approach preclude the possibility of simulating directly flows with Re $\gg 100$. To test whether Fickian behavior persists at higher Re, a subgrid model [21] was utilized with a Smagorinsky constant, $C_s = 0.1$. In this approach a space-filtered particle distribution is defined those dynamics are governed by a LBM with a space-dependent relaxation time. Using this subgrid model a flow with Re$\sim$2200 was simulated. The dispersion of a tracer, due to the resolved scales of turbulent fluid motions, was found to remain Fickian in the far field. Consequently, if a transition to anomalous dispersion does occur then it is predicted to occur at larger Re.

V. MEASURED AND PREDICTED MEAN CONCENTRATIONS

Flow within the experimental packed bed is predicted to have Re$\approx$113 and Re$'\approx$5.4 and be chaotic (weakly turbulent). Replicate profiles of mean concentrations measured 20 mm beneath the first layer of spheres are shown in Fig. 9. The replicates were made at 24 h intervals during which time the air flow through the packed bed was maintained. The source of the scatter in the experimental data is unclear but could indicate that very-low-frequency components are present in the flow.

A comparison of predicted and ensemble average (over the six replicates) measured concentrations is shown in Fig. 10. The measurements were made beneath the packed bed in the wakes generated by the spheres in the first layer. This accounts for the nonvanishing measured concentrations in locations directly beneath the spheres. In contrast and because of the imposition of periodic boundary conditions, model predictions are shown for locations within the plane containing the lower poles of the spheres in the first layer. To account for the difference between volumes of free space beneath the packed bed in the experiment and the void volumes between the spheres in the computational domain, predicted concentrations have been reduced by a factor $A_v/A_\triangle = 1 - \pi/(2\sqrt{3})$, where A_v is the cross-sectional area of a void formed between three neighboring spheres in the appropriate horizontal plane and $A_\triangle$ is the area of the triangle defined by the centers of these spheres. In spite of these differences, it is seen that the agreement between measured and predicted mean concentrations is very good. Particularly well predicted is the extent of the dispersion and the gradients concentration.

VI. CONCLUSIONS

This paper has reported numerical studies of fluid flow through a close-packed bed of spheres and on experimental

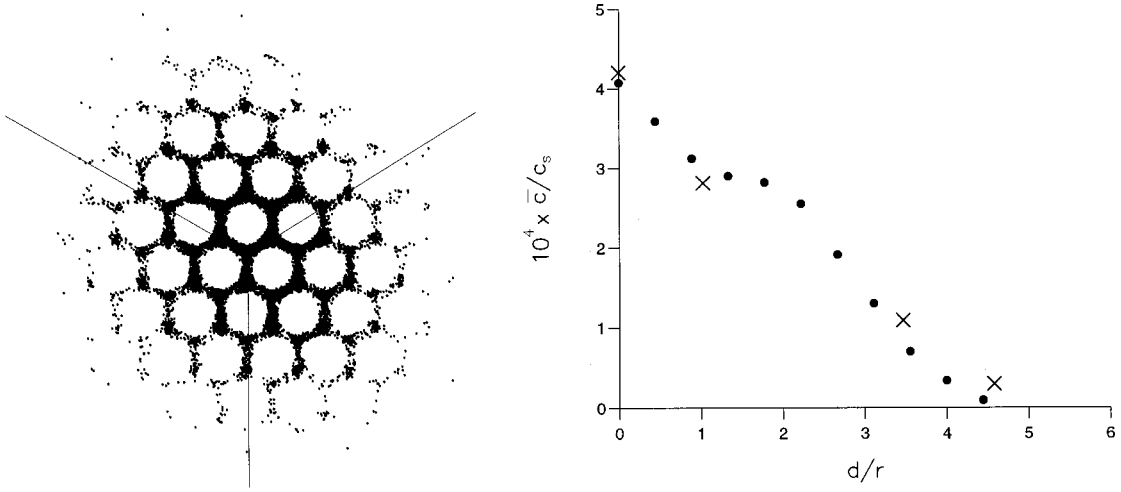

FIG. 10. A comparison of ensemble-averaged measured concentrations (●) 20 mm below the lower poles of the spheres in the first layer and predicted (×) volume-averaged concentrations in the plane containing the lower poles of the spheres in the first layer. The line and its symmetry equivalents along which the measurements and predictions were made is indicated. Distances d are measured from the central sphere and have been rendered nondimensional using the sphere radius r. Also shown (left) are the locations in the plane containing the lower poles of the spheres in the first layer through which the simulated trajectories of tracer particles passed. The source strength is denoted by c_s. Measured concentrations are accurate to within $\pm 2\%$.

and numerical studies of tracer-particle dispersion. The normalized local kinetic energy of the steady flow, which exists at low Reynolds numbers, $Re<14$, is predicted to have a power-law distribution. This indicates that the stagnant zones play a significant role in transport through the packed bed and so provides a three dimensional companion for the two-dimensional counterexample to the paradigm of electrical flow in random resistor networks and transport of mass and momentum in disordered porous media [15].

The steady flow is predicted to become unsteady at $Re \sim 14$, resulting in time-periodic oscillations in the component of velocity parallel to the direction of the gradient in applied pressure. At $Re \sim 20$, the transverse components of velocity are predicted to fluctuate, resulting in quasiperiodicity for $Re>22$ and eventually chaos at $Re \sim 40$. It was suggested that this sequence of transitions, but not the critical Reynolds numbers, is independent of the direction of the gradient in applied pressure. The normalized local kinetic energy of the chaotic flow has a log-normal distribution in analogy with the log-binomial distribution of local currents in the analogous electrical transport problem [16,17]. Consequently, the kinetic energy distribution cannot be characterized by a unique velocity scale.

Tracer dispersion in the flows with fluctuating transverse velocity components is predicted to be Fickian in the far field and so, contrary to most cases of dispersion in inhomogeneous turbulent flows, can be described by a diffusion model. Model predictions for tracer-particle dispersion in a chaotic flow with $Re \sim 100$ were found to be in close agreement experiment.

ACKNOWLEDGMENTS

This work was supported by the BBSRC through ROPA Grant No. 978945. Special thanks goes to Mr. Terry Layton and Mr. John Tilcock for their assistance in the design and construction of the experimental rig. Dr. A. M. Reynolds would also like to thank Reghan Hill of Cornell University for many helpful discussions on his application of the lattice-Boltzmann method through spheres in close-packed arrangements.

[1] H. C. Brinkman, Appl. Sci. Res., Sect. A **1**, 27 (1947).
[2] H. Hasimoto, J. Fluid Mech. **5**, 317 (1959).
[3] D. L. Koch and J. F. Brady, J. Fluid Mech. **154**, 399 (1985).
[4] D. L. Koch and J. F. Brady, J. Fluid Mech. **180**, 387 (1986).
[5] T. H. Wegner, A. J. Karabelas, and T. J. Hanratty, Chem. Eng. Sci. **26**, 59 (1971).
[6] R. J. Hill and D. L. Koch, Bull. Am. Phys. Soc. **44(8)**, 69 (1999).
[7] D. L. Koch and A. J. C. Ladd, J. Fluid Mech. **349**, 31 (1997).
[8] A. J. C. Ladd, J. Fluid Mech. **271**, 311 (1994).
[9] Y. H. Qian, D. d'Humieres, and P. Lallemand, Europhys. Lett. **17**, 479 (1992).
[10] S. Chen and G. D. Doolen, Annu. Rev. Fluid Mech. **30**, 329 (1998).
[11] J. M. Buick, Ph.D. thesis, University of Edinburgh, UK, 1997 (unpublished).
[12] I. Ginzbourg and P. M. Adler, J. Phys. II **4**, 191 (1994).
[13] D. R. Noble, S. Y. Chen, J. G. Georgiadis, and R. O. Buckius, Phys. Fluids **7**, 203 (1995).
[14] D. Kandhai, A. Koponen, A. Heokstra, M. Kataja, J. Timonen, and P. M. A. Sloot, J. Comput. Phys. **150**, 482 (1999).
[15] J. S. Andrade, Jr., M. P. Almeida, J. Mendes Filho, S. Havlin, B. Suki, and H. E. Stanley, Phys. Rev. Lett. **20**, 3901 (1997).
[16] L. de Arcangelis, S. Redner, and A. Coniglio, Phys. Rev. B **31**, 4725 (1985).
[17] L. de Arcangelis, S. Redner, and A. Coniglio, Phys. Rev. B **34**, 4656 (1986).
[18] R. J. Hill (private communication).
[19] J. C. R. Hunt and J. C. Vassilicos, Proc. R. Soc. London, Ser. A **343**, 183 (1991).
[20] D. L. Koch, R. J. Hill, and A. S. Sangani, Phys. Fluids **10**, 3035 (1998).
[21] S. Hou, J. Sterling, S. Chen, and G. D. Doolen, Fields Inst. Commun. **6**, 151 (1996).